



# UNIVERSITÀ DI PARMA

## ARCHIVIO DELLA RICERCA

University of Parma Research Repository

The influence of laser welding configuration on the properties of dissimilar stainless steel welds

This is the peer reviewed version of the following article:

*Original*

The influence of laser welding configuration on the properties of dissimilar stainless steel welds / Romoli, Luca; Rashed, C. A. A.. - In: INTERNATIONAL JOURNAL, ADVANCED MANUFACTURING TECHNOLOGY. - ISSN 0268-3768. - 81:1-4(2015), pp. 563-576. [10.1007/s00170-015-7234-8]

*Availability:*

This version is available at: 11381/2815551 since: 2021-10-18T10:14:04Z

*Publisher:*

Springer London

*Published*

DOI:10.1007/s00170-015-7234-8

*Terms of use:*

Anyone can freely access the full text of works made available as "Open Access". Works made available

*Publisher copyright*

note finali coverpage

(Article begins on next page)

## Dear Author

Here are the proofs of your article.

- You can submit your corrections **online**, via **e-mail** or by **fax**.
- For **online** submission please insert your corrections in the online correction form. Always indicate the line number to which the correction refers.
- You can also insert your corrections in the proof PDF and **email** the annotated PDF.
- For **fax** submission, please ensure that your corrections are clearly legible. Use a fine black pen and write the correction in the margin, not too close to the edge of the page.
- Remember to note the **journal title**, **article number**, and **your name** when sending your response via e-mail or fax.
- **Check** the metadata sheet to make sure that the header information, especially author names and the corresponding affiliations are correctly shown.
- **Check** the questions that may have arisen during copy editing and insert your answers/corrections.
- **Check** that the text is complete and that all figures, tables and their legends are included. Also check the accuracy of special characters, equations, and electronic supplementary material if applicable. If necessary refer to the *Edited manuscript*.
- The publication of inaccurate data such as dosages and units can have serious consequences. Please take particular care that all such details are correct.
- Please **do not** make changes that involve only matters of style. We have generally introduced forms that follow the journal's style.
- Substantial changes in content, e.g., new results, corrected values, title and authorship are not allowed without the approval of the responsible editor. In such a case, please contact the Editorial Office and return his/her consent together with the proof.
- If we do not receive your corrections **within 48 hours**, we will send you a reminder.
- Your article will be published **Online First** approximately one week after receipt of your corrected proofs. This is the **official first publication** citable with the DOI. **Further changes are, therefore, not possible.**
- The **printed version** will follow in a forthcoming issue.

### Please note

After online publication, subscribers (personal/institutional) to this journal will have access to the complete article via the DOI using the URL:

<http://dx.doi.org/10.1007/s00170-015-7234-8>

If you would like to know when your article has been published online, take advantage of our free alert service. For registration and further information, go to:

<http://www.link.springer.com>.

Due to the electronic nature of the procedure, the manuscript and the original figures will only be returned to you on special request. When you return your corrections, please inform us, if you would like to have these documents returned.

**Metadata of the article that will be visualized in OnlineFirst**

---

Please note: Images will appear in color online but will be printed in black and white.

---

1	Article Title	<b>The influence of laser welding configuration on the properties of dissimilar stainless steel welds</b>	
2	Article Sub- Title		
3	Article Copyright - Year	<b>Springer-Verlag London 2015 (This will be the copyright line in the final PDF)</b>	
4	Journal Name	The International Journal of Advanced Manufacturing Technology	
5		Family Name	<b>Romoli</b>
6		Particle	
7		Given Name	<b>L.</b>
8	Corresponding	Suffix	
9	Author	Organization	University of Parma
10		Division	Department of Industrial Engineering
11		Address	Parma, Italy
12		e-mail	luca.romoli@unipr.it
13		Family Name	<b>Rashed</b>
14		Particle	
15		Given Name	<b>C. A. A.</b>
16		Suffix	
17	Author	Organization	Shahjalal University of Science and Technology
18		Division	Department of Industrial and Production Engineering
19		Address	Shahjalal, Bangladesh
20		e-mail	
21		Received	8 January 2015
22	Schedule	Revised	
23		Accepted	26 April 2015
24	Abstract	Laser beam welding of dissimilar ferritic/martensitic stainless steels was performed in constrained butt joint configuration with the objective of identifying the influence of the melting ratio between the two base metals on the ultimate shear strength of the welds. Based on a full factorial design, experiments demonstrated that varying the incidence angle up to 45° and offsetting the focal position with respect to the materials' interface within the limits imposed by the laser spot diameter are a reliable method to control	

the melting ratio and maintaining the expected resistance length at the material interface. The weld configuration parameters were correlated by means of the analysis of variance (ANOVA) method with shear resistance length and the melting ratio: the incidence of surface cracks can be significantly reduced increasing the ferritic steel area, involved in the formation of seam, over 60 % of the whole melt zone. Push-out tests performed on the specimens revealed that such a configuration has beneficial aspects on the ultimate shear strength of the seam meaning that the prevailing effect is the decreased brittleness of the weld by decreasing its carbon content under 0.5 % in weight.

- 
- |    |                                |   |
|----|--------------------------------|---|
| 25 | Keywords<br>separated by ' - ' | Laser welding - Dissimilar steels - Melting ratio |
|----|--------------------------------|---|
- 
- |    |                          |  |
|----|--------------------------|--|
| 26 | Foot note<br>information |  |
|----|--------------------------|--|

# The influence of laser welding configuration on the properties of dissimilar stainless steel welds

L. Romoli<sup>1</sup> · C. A. A. Rashed<sup>2</sup>

Received: 8 January 2015 / Accepted: 26 April 2015  
© Springer-Verlag London 2015

**Abstract** Laser beam welding of dissimilar ferritic/martensitic stainless steels was performed in constrained butt joint configuration with the objective of identifying the influence of the melting ratio between the two base metals on the ultimate shear strength of the welds. Based on a full factorial design, experiments demonstrated that varying the incidence angle up to 45° and offsetting the focal position with respect to the materials' interface within the limits imposed by the laser spot diameter are a reliable method to control the melting ratio and maintaining the expected resistance length at the material interface. The weld configuration parameters were correlated by means of the analysis of variance (ANOVA) method with shear resistance length and the melting ratio: the incidence of surface cracks can be significantly reduced increasing the ferritic steel area, involved in the formation of seam, over 60 % of the whole melt zone. Push-out tests performed on the specimens revealed that such a configuration has beneficial aspects on the ultimate shear strength of the seam meaning that the prevailing effect is the decreased brittleness of the weld by decreasing its carbon content under 0.5 % in weight.

**Keywords** Laser welding · Dissimilar steels · Melting ratio

## 1 Introduction

The recent advancement in manufacturing technology is increasing the demand for dissimilar metal welding. Joints between components of different material or compositions are commonly used in the power generation, chemical, petrochemical, nuclear, automobiles, and electronics industries [1]. The ability to use different metals and compositions in a product provides the designer and production engineer with greater flexibility and often results in technical and economic advantages over components manufactured from a single material. Many problems are also associated to the topic of dissimilar welding, depending on the metals being joined and the process employed. In the welding of dissimilar metals, the different chemical, metallurgical, and physical properties such as thermal conductivity, thermal expansion coefficient, and melting point should be taken into consideration [2]. The formation of detrimental metallurgical phases in these welds could result in decrease in mechanical and functional properties of the joint. The difference between the physical properties of the two metals to be welded leads to an asymmetry in heat and fluid flow which in turn directs to the development of unique features in the weld microstructure [3]. Thus, solidification microstructures, the asymmetric shape of the weld, and mixing patterns need special attention. Among the available welding techniques, laser welding (high specific power and low-energy input process) is emerging as a valid and promising alternative for joining of dissimilar metal, as it provides solutions to a number of problems encountered with conventional techniques [4].

Laser welding provides several advantages, such as higher productivity, better weld quality with narrow heat-affected zone (HAZ), lower distortions, and higher flexibility over the conventional processes [5]. The weld quality mainly depends on the mechanical properties, weld bead geometry, and

✉ L. Romoli  
luca.romoli@unipr.it

<sup>1</sup> Department of Industrial Engineering, University of Parma, Parma, Italy

<sup>2</sup> Department of Industrial and Production Engineering, Shahjalal University of Science and Technology, Shahjalal, Bangladesh

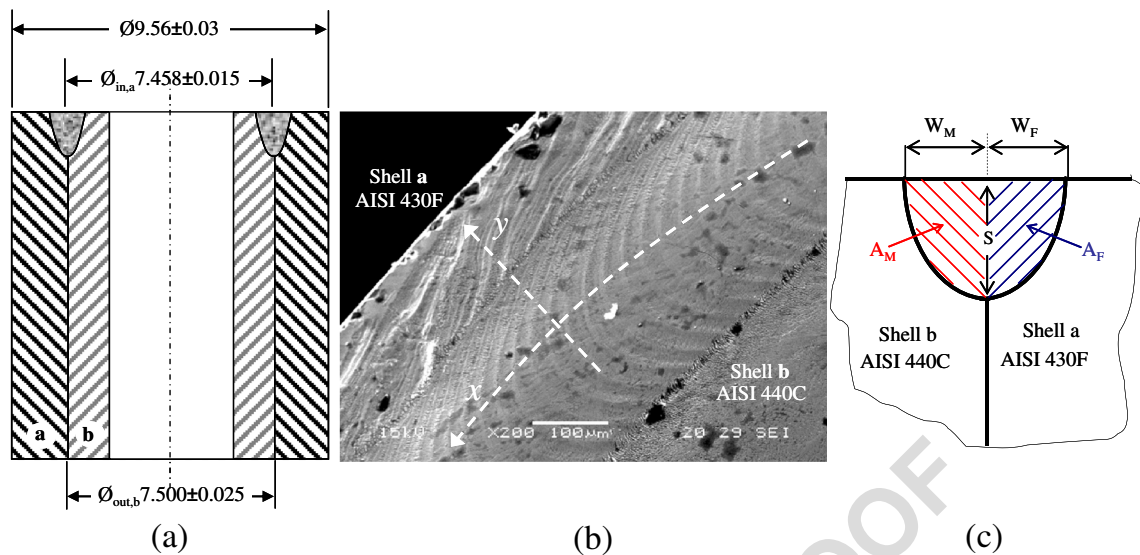


**Fig. 1** a Draft of a typical axial section of the welded components with relative dimensions. b Top SEM view of a dissimilar butt welded surface at the intersection of AISI 430F and AISI 440C:  $x$ -axis is circular and set at the material interface, and  $y$ -axis is positive in the direction of AISI

430F. c Theoretical weld bead profile and its geometrical features ( $W_M$ : martensitic weld width,  $W_F$ : ferritic weld width,  $S$ : resistance length) together with the areas of both material intersected by the weld ( $A_M$ : supposed martensitic weld area,  $A_F$ : supposed ferritic weld area)

65 distortion of the welded joint. All of these quality characteristics are directly related to welding parameters. Several efforts  
66 have been done to understand the mechanical and microstructural behavior of dissimilar metal welds and to optimize the  
67 welding processes used.

68 Phanikumar et al. [3] investigated the continuous welding of iron and copper using a laser heat source. The microstructural  
69 analysis at different process conditions of the weld/base-metal interface shows features that are different on the two  
70 sides of the weld. Vaidya et al. [6] used Nd:YAG laser for dissimilar butt welding of aluminum AA6056 and titanium  
71 Ti6Al4V alloy without using a filling wire. In their study, the interfacial area was decreased that resulted in decreased reaction  
72 zone, improved interfacial binding, reduced the grain size in the fusion zone, no segregation of grain boundary, and  
73 refined microstructure with improved properties. Homogeneous microstructure of the weld metal and very few weld  
74 defects were observed in butt welding of two different thickness stainless steel plates [7].

75 Caiazzo et al. [8] studied the autogenous disk laser welding of dissimilar metals commonly used in aerospace applications.  
76 They provided a comprehensive description of the quality

77 issues in terms of both structure and shape defects, via nondestructive tests and dimensional checks by optimizing three  
78 factor experimental plans with power, welding speed, and beam angle. Gao et al. [9] developed the laser keyhole  
79 welding of titanium and magnesium alloys and showed that the offset, i.e., the change of incident laser beam position,  
80 plays the significant role on joint properties by the change of the power density irradiated at the Ti–Mg initial interface.  
81 However, the variation of the beam position was not found to be a less significant factor for the weld geometry in keyhole  
82 mode of dissimilar austenitic-martensitic stainless steel [10].

83 The attention paid by researchers on the weld geometry testifies its influence on the mechanical properties of the  
84 welded joints and, consequently, on the related welding quality. Liao et al. [11] studied the effects of pulse energy  
85 and incident angle on the cross-sectional size and shape of the welded bead. Their study illustrated that laser incidence  
86 angle along with the laser energy is an important parameter for controlling the geometry of the welded spot.

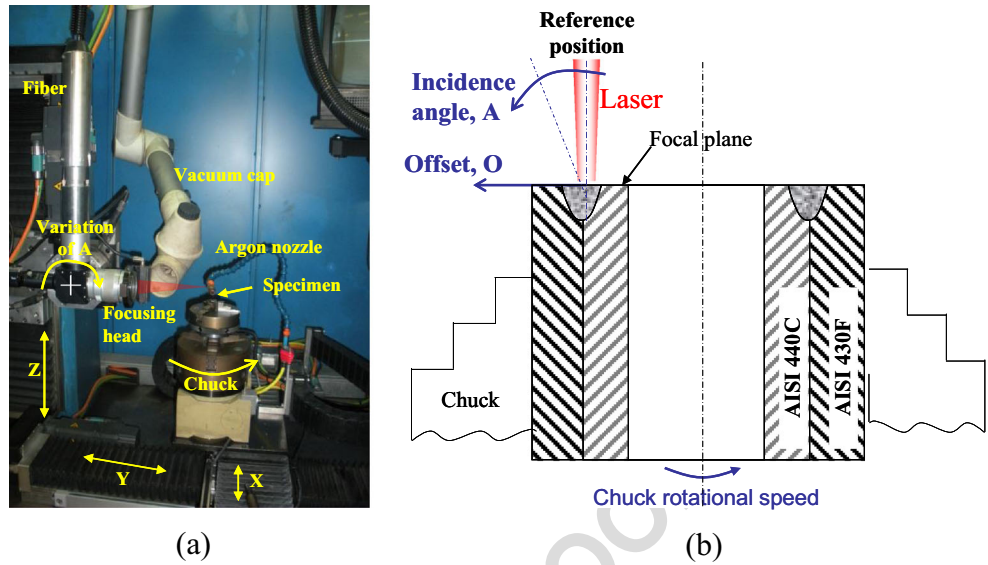
87 Weld material, joint configuration, and welding parameters have significant effects on the weld seam characteristics,  
88 on the weld microstructure, on the presence of defects, and on the effective mechanical properties of the whole joint.  
89 To optimize the welding parameters and to obtain proper welding geometry, various methods of obtaining the desired  
90 output variables throughout model development can be used. Among these, design of experiment (DOE) may be the  
91 most efficient way for a systematic study as it grown rapidly by its diversified application in different areas of  
92 manufacturing. Benyounis and Olabi [12] reported a literature review

t1.1 **Table 1** Average chemical composition of AISI 440C and AISI 430F steels

t1.2		%C	%Mn	%Si	%Cr	%S	%Mo
t1.3	AISI 440C	0.95-1.2	1.00	1.00	16.0–18.0	Max 0.03	0.6
t1.4	AISI 430F	0.12	1.25	1.00	16.0–18.0	Min 0.15	0.75



**Fig. 2** a Photographic view of Nd:YAG laser welding system. b Cross section of the joined components: welding configuration varies from the reference position (beam axis orthogonal to the surface, pointing the intersection of AISI 430F and AISI 440C) with the use of input parameters



118 on various optimization methods; those are applied to  
 119 define the desired output variables through developing  
 120 mathematical models. Anawa and Olabi [13] showed  
 121 that ferritic/austenitic welded joints have better mech-  
 122 anical properties compared to base metals by the minimi-  
 123 zation of laser power and maximization of welding  
 124 speed by the application of the Taguchi approach.  
 125 Ruggiero et al. [14] optimized the weld bead geom-  
 126 etry and investigated the effect of laser power, welding  
 127 speed, and focal point position on the operating cost  
 128 using response surface methodology (RSM). Khan  
 129 et al. [15] also used RSM to optimize the welding pa-  
 130 rameters (welding speed, laser power, laser incidence  
 131 angle, and defocus distance) in ferritic/austenitic stain-  
 132 less steel to obtain the most desirable weld quality in  
 133 terms of weld bead geometry under predefined mech-  
 134 anical strength requirements.

135 The laser welding mode (conduction or keyhole) affects the  
 136 size of the fusion zone, as the dilution between two base  
 137 metals strongly depends on the laser energy supply to the

materials. Marashi et al. [16] showed that the failure behavior  
 of the fusion zone of dissimilar stainless steel is controlled by  
 the dilution between two base metals. Dissimilar welding of  
 low carbon to austenitic stainless steel sheets resulted in asym-  
 metric shape of the fusion zone as different materials having  
 different thermal conductivities [17].

From the above literature, it is clear that laser welding is a  
 suitable technique for joining dissimilar metals and explains  
 the reasons of its increasing use also in the field of thin-walled  
 pressure vessels for biomedical and automotive applications  
 [18]. Indeed, high-strength metal cylinders can be capped with  
 a dissimilar metal of various shapes to increase the corrosion  
 properties of the component (e.g., in surgery devices) or to  
 enhance the wear resistance (e.g., parts of valves for precision  
 mechanics), etc.

The extremely precise and intense energy concentration  
 obtainable by modern fiber sources allows for numerous weld  
 configurations at the metal interface. Among all, butt welding  
 is the one which enables an easier control of the mixing be-  
 tween the two dissimilar steels in the melt pool [19].

**Table 2** Technical specification of the laser welding process

Parameter	Value
Laser source	Fiber laser
Laser power (W)	800
Fiber diameter (mm)	0.4
Collimating (mm)	200
Focusing (mm)	200
Welding speed (mm/s)	65
Shielding gas type	Argon
Shielding gas flow rate (l/min)	6

**Table 3** Experimental conditions and response factors

Process factors	Tested values				Response factors
<i>O</i> offset (μm)	0	100	200		Resistance length (S)
<i>A</i> incidence angle (°)	0	15	30	45	Melting ratio (MR)
Constant factors					
Base material	Outer shell	AISI 430F			
	Inner shell	AISI 440C			

t4.1 **Table 4** Design matrix with actual factors and measured mean responses

t4.2	Standard order	Process factors		Response factors	
t4.3		$O$ ( $\mu\text{m}$ )	$A$ (deg)	MR (a.u.)	$S$ ( $\mu\text{m}$ )
t4.4	1	0	0	0.8	760
t4.5	2	100	0	2.0	695
t4.6	3	200	0	2.7	465
t4.7	4	0	15	0.5	535
t4.8	5	100	15	1.6	610
t4.9	6	200	15	2.2	450
t4.10	7	0	30	0.3	480
t4.11	8	100	30	0.6	550
t4.12	9	200	30	1.5	590
t4.13	10	0	45	0.1	280
t4.14	11	100	45	0.3	415
t4.15	12	200	45	0.6	455

## 2 Materials and experimental procedures

176

### 2.1 Materials and weld design

177

Experiments are performed in butt constrained circular seam to replicate the weld configuration of a pressure vessel. The draft in Fig. 1a shows the welding configuration together with the specimens' diameters and their coupling. The internal tubular shell is made of martensitic stainless steel AISI 440C (prehardened and tempered) and is assembled with the external one made of ferritic stainless steel AISI 430F (cold drawn, annealed, and centerless ground). The selected materials are frequently used both in automotive and biomedical applications according to peculiar design criteria which impose high hardness and good resistance to corrosion as well. Table 1 reports the chemical composition of the used steels.

The inside diameter of the outer shell and the outside diameter of the seat are machined to  $\text{Ø}7.500 \pm 0.025$  mm and  $\text{Ø}7.458 \pm 0.015$  mm, respectively, to have a clearance fit between them when the shells are assembled.

The geometrical features characterizing the weld seam profile are defined in Fig. 1:  $W_M$  represents the weld width on the martensitic material while  $W_F$  represents the one on the ferritic stainless steel. The ultimate shear strength of the weld is guaranteed by the length of the melt pool at the material interface, here defined as resistance length  $S$ , since the joint is supposed to fail under the action of disassembly forces parallel to the shells' axis.

In order to consider only the influence of the welding configuration on the melt pool geometry and its composition (between the dissimilar steels), the weld seams obtained in this study are performed with the following laser parameters: laser power of 800 W, welding speed of 65 mm/s, and spot diameter of 0.4 mm. This combination results in an energy density (ED calculated as the ratio between the input power and the product of welding speed and spot diameter) supply to the specimen of about  $30 \text{ J/mm}^2$ . Nevertheless, the findings of this research can be also applied to different combinations of laser

158 Main purpose of the present research is, in fact, to go beyond the already studied influence of process parameters on the weld bead and, then, to identify a reproducible setup for a common laser welding cell to control the melting ratio between two parent metals. The effects of welding parameters like laser beam position (with respect to the materials' interface) and incidence angle (with respect to the materials' irradiated surface) on the weld profile will be studied by means of a structured DOEs. An attempt based on full factorial design will be proposed to mathematically link the parameters determining the butt welding configuration with the geometry of the melt pool and the melting ratio of two dissimilar metals. This step is retained a technical key factor to determine how mixing two different materials could enhance the mechanical properties of the single base metals in butt-welded joints. At this purpose, the final objective is to perform disassembly tests on the obtained joints in order to detect the influence of melting ratio on the ultimate shear strength of the welds.

**Fig. 3** Cross sections of welds in a reference position  $O=0, A=0^\circ$  and **b**  $O=200 \mu\text{m}, A=45^\circ$ . Cross section (a) reports the martensitic area  $A_M$  inside the red-dashed contour and the ferritic area  $A_F$  inside the blue-dashed contour

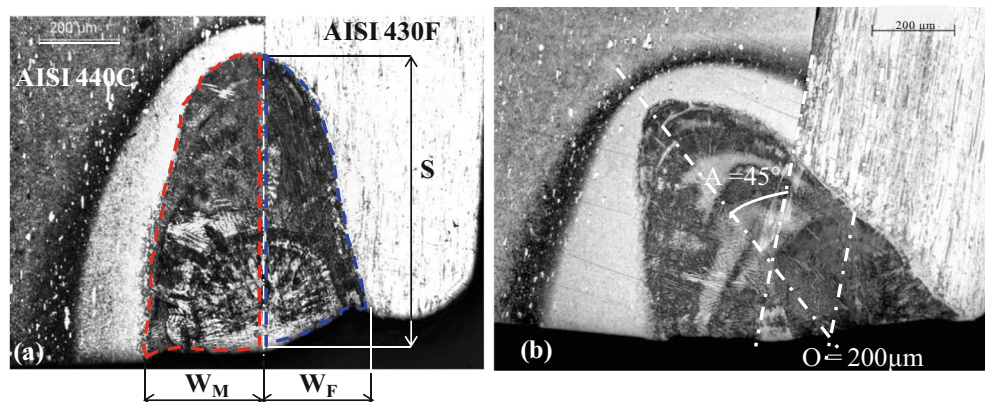
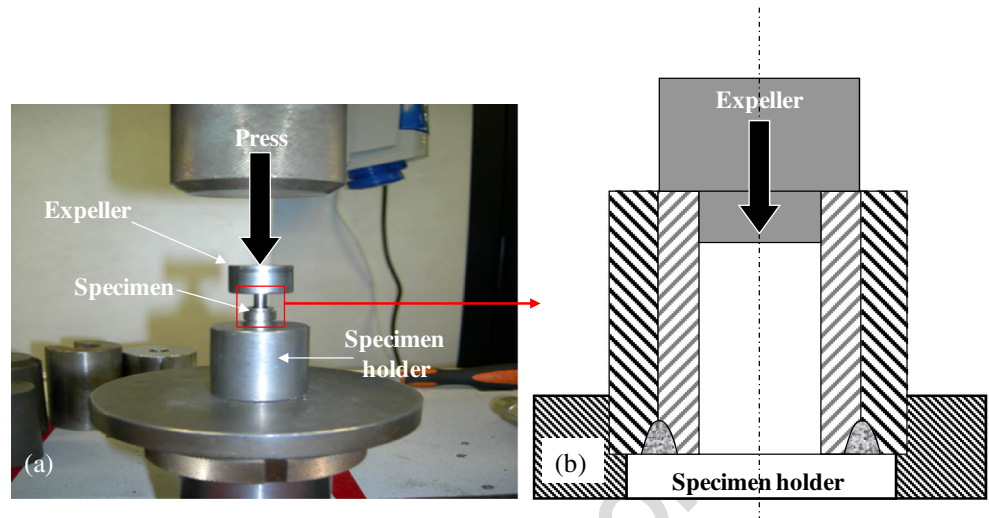




**Fig. 4** **a** View of the experimental setup for the push-out test of the weld. **b** Cross-sectional draft of the specimen



212 parameters under the condition that the heat transfer is conduction dominated (up to 50–60 J/mm<sup>2</sup> according to [20]).  
 213 Heat exchanges established under the formation of a plasma channel (as in keyhole welding mode) produce much higher  
 214 thermal transients, thus generating a remarkably different microstructure of the weld with respect to those observable when  
 215 the weld is conduction dominated.

216 However, even using low values of ED supply on the  
 217 steels, the experimental practice often reports the occurrence of microcracks on the seam. These defects are  
 218 supposed to grow up during the solidification process in zones where the mixing of the two metals with

224 different chemical composition and thermal properties  
 225 is less homogeneous. Microcracks can be classified according to the ISO 13919-1:1996 [21] standard.

226 To reduce the incidence of crack formation, which testifies the embrittlement of the weld seam and mostly develops on  
 227 the side of the martensitic steel, it is here hypothesized to change the position of the laser beam toward the ferritic steel,  
 228 by offsetting the beam axis with respect to the interface of the two materials.

229 Nevertheless, increasing the beam offset *O* (along *y*-axis in Figs. 1b and 2b) may result in a drastic decrease of the resistance length (up to the value for which the melt pool does not involve the martensitic steel) with a consequent decay in the ultimate shear strength. To avoid this severe limitation and, at the same time, to obtain a weld profile less prone to cracking, the beam incidence angle *A* (see Fig. 2b) has to be varied as well. This results in the need of defining weld cross-sectional geometries for each combination (*O*; *A*) adopted.

230 Inclining the laser beam has a further beneficial effect of increasing the irradiated area which becomes elliptical (increasing *A*) with the longer axis disposed along *y*-direction. The elongation of the irradiated area allows for a reduction of the thermal gradient in *y*-direction which may contribute to a less severe thermal cycle on the extinction zones of the weld bead, where microcracks usually appear.

231 For each combination of (*O*; *A*), the melting ratio between the two dissimilar steels is supposed to vary, thus influencing the microstructural properties of the weld bead and the occurrence of surface cracking, as also stated in [22]. The melting ratio can be defined by analyzing the cross section of the welds as the ratio between the areas of ferrite and martensite involved in the melt pool, as shown in Eq. (1):

$$MR = \frac{A_F}{A_M} \tag{1}$$

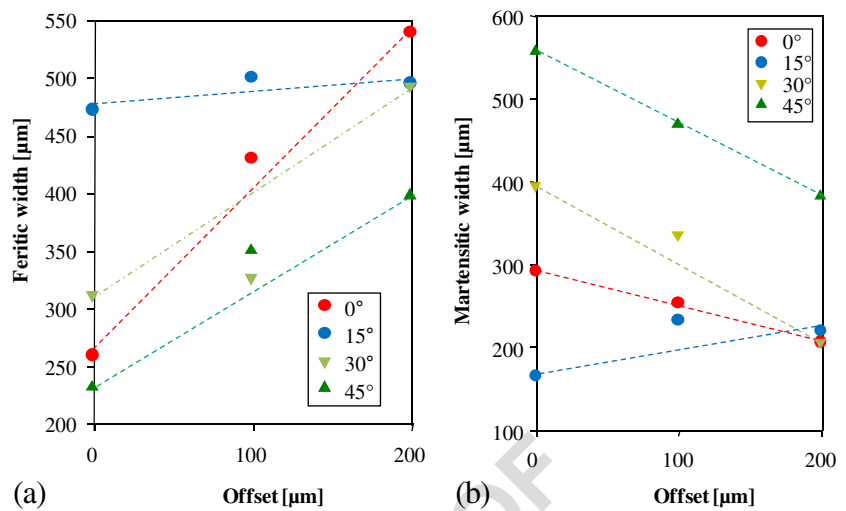
t5.1 **Table 5** Occurrence of surface microcracks on the weld seam with respect to the analyzed weld geometries

t5.2	Welding configuration	Offset, <i>O</i> (μm)	Incidence angle, <i>A</i> (°)	Surface cracks <sup>a</sup>
t5.3	1	0	0	1
t5.4	2	100	0	0
t5.5	3	200	0	0
t5.6	4	0	15	3
t5.7	5	100	15	0
t5.8	6	200	15	0
t5.9	7	0	30	3
t5.10	8	100	30	2
t5.11	9	200	30	0
t5.12	10	0	45	3
t5.13	11	100	45	3
t5.14	12	200	45	2

Values are attributed according to ISO 13919-1:1996 [17], after inspection on the three samples for each configuration

<sup>a</sup> 0=no defects, 1=exist but acceptable, 2–3=not acceptable

**Fig. 5** Measurement of **a** ferritic width and **b** martensitic width for different offset positions and different incident angles. The dashed lines are guide to show the trend



where MR is the melting ratio,  $A_F$  is the area of ferrite, and  $A_M$  is the area of martensite. In the perspective of reducing the incidence of crack formation up to a less dangerous value for the strength of the weld, a more favorable configuration provides larger ferritic area, resulting in higher melting ratio.

This calculation implies the hypothesis of a homogeneous mixing of the two dissimilar steels in the melt pool. As a matter of fact, the melting process is associated with the formation of convective flows [23] (especially Marangoni flows). In case of weld of different steels, this induces a chemical composition homogenization of the melting pool volume. Obviously, some nonhomogeneity could be present, especially in the regions close to the HAZ, but their effects on weld properties are proportional to their extensions, thus almost negligible with respect to the melting pool volume.

Positioning the focal point at the material interface, avoiding any possible misalignment, is extremely important for the described experimental setup. This is obtained by a specifically conceived sharp-pointed jig which is mounted on the optical head and allows for positioning by real contact the head at the material interface at the exact focal distance.

## 2.2 Experimental procedures

Specimens are clamped and centered in a chuck providing the rotational speed. They are then welded circularly in a butt joint configuration using a continuous wave Rofin fiber laser (maximum power 1 kW). The optical system consisted of a 0.4-mm fiber and two lenses of 200-mm focal and collimate lengths which enable to deliver the laser with a minimum focal spot

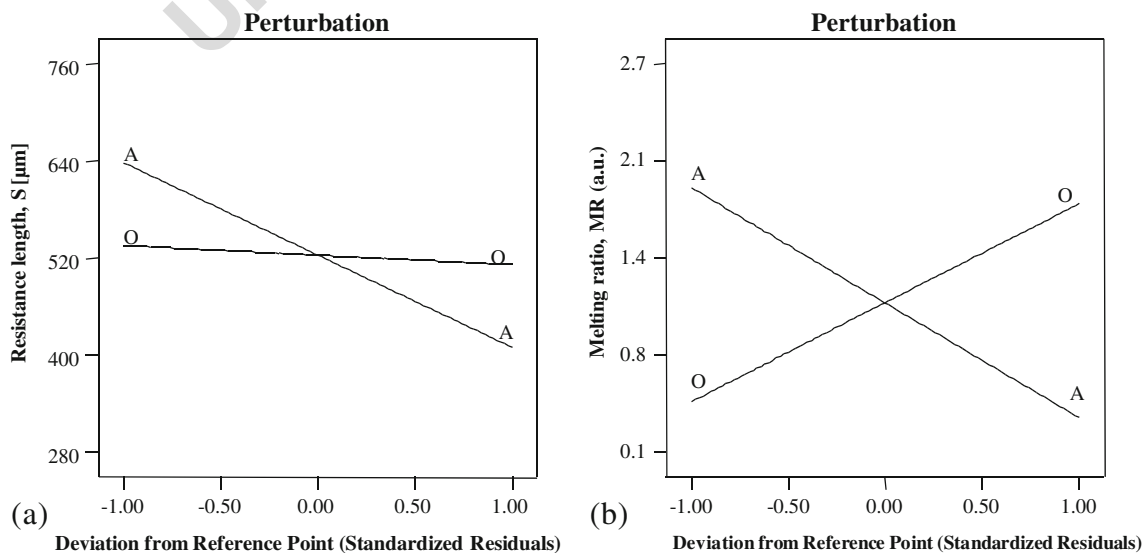
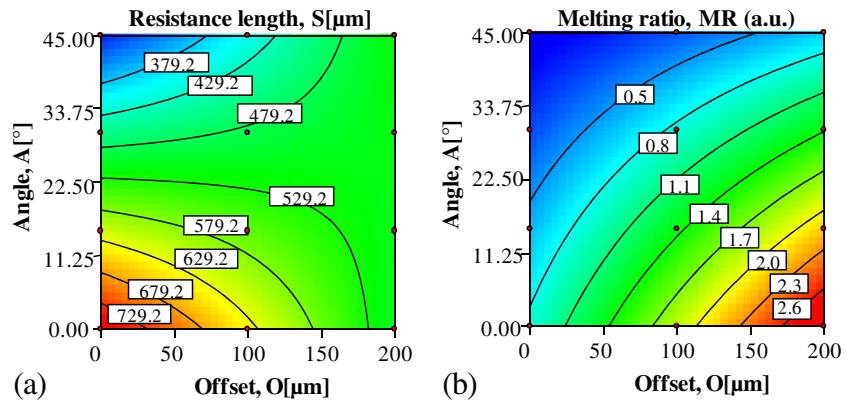


**Fig. 6** Perturbation plots showing effects of all factors on **a** resistance length and **b** melting ratio

**Fig. 7** Contour graphs showing the interaction effects of  $O$  and  $A$  on **a** resistance length and **b** melting ratio



286 diameter of 0.4 mm. The technical details of the employed  
287 laser welding process are shown in Table 2.

288 During experimentation,  $O$  and  $A$  are selected as process  
289 input variables for the laser welding based on statistical factor-  
290 ial experimental design with full replication. Table 3 shows  
291 the experimental conditions, laser welding input variables,  
292 and design levels used at a glance. The working range for  
293 the incident angle is brought to the upper limit of  $45^\circ$ , for  
294 which the highest reflection is expected, while only three steps  
295 are hypothesized for the offset,  $O$ . This is done to avoid insuf-  
296 ficient melt of the martensitic steel, as testified by a prelimi-  
297 nary set of experiments conducted with  $O=300 \mu\text{m}$ .

298 General full factorial design is utilized as a statistical DOE  
299 technique. Full factorial DOE technique relates the welding  
300 input parameters to each of the two output responses of the  
301 weld (resistance length and melting ratio). Later, the process  
302 factors are used as input parameters to develop a mathematical  
303 model which links them to the ultimate shear strength of the  
304 performed welds. Analysis of variance (ANOVA) and other  
305 adequacy measures are used to measure the correctness of the  
306 models developed and their significant linear and interaction  
307 model terms. Table 4 shows the measurement of the averaged  
308 value of response parameters for different laser welding  
309 conditions.

310 Argon is used as shielding gas with a constant flow rate of  
311 6 l/min to protect weld surface from oxidation and suppresses

the generation of plasma during welding. A standard ultra- 312  
sound washing procedure is followed to clean, cool, and dry 313  
the specimens. The experimental setup for laser welding sys- 314  
tem is shown in Fig. 2a. 315

**2.3 Weld bead characterization** 316

After welding, seam cross sections are prepared by cutting the 317  
samples axially using SampleMet II (Beuhler, IL) model abra- 318  
sive cutter. The sectioned samples are mounted, polished, and 319  
chemically etched by immersion in Vilella reagent for micro- 320  
structural characterization. Leica IM500 software, incorporat- 321  
ed in an optical microscope (Leica MZ125), is used to mea- 322  
sure resistance length, martensitic and ferritic weld width, and 323  
the area of ferrite and martensite needed to calculate the melt- 324  
ing ratio according to Eq. 1. 325

Experiments are replicated six times for each welding combi- 326  
nation ( $A; O$ ) to produce three specimens to be cut for met- 327  
allographic analysis and three for the mechanical characteri- 328  
zation of the weld (see Sect. 2.4). Figure 3 reports the typical 329  
cross section at the reference position and at the extreme 330  
values of the parameter tested range. 331

The guidance on quality levels for imperfections given in 332  
ISO 13919-1:1996 [21] is followed to ensure the desired weld 333  
quality in terms of surface cracking. At this point, each welded 334  
specimen is visually inspected using the optical microscope. 335

t6.1 **Table 6** Sequential model sum  
t6.2 of squares for resistance length  
model

Source	Sum of squares	df	Mean square	F value	P value	Prob>F
Mean	3.292E+006	1	3.292E+006	—	—	—
Linear	88148.54	2	44074.27	4.11	0.0538	
2FI	64400.62	1	64400.62	16.10	0.0039	Suggested
Quadratic	13236.46	2	6618.23	2.12	0.2017	
Cubic	15963.75	3	5321.25	5.69	0.0936	Aliased
Residual	2806.87	3	935.62	—	—	—
Total	3.476E+006	12	2.897E+005	—	—	—

t6.3  
t6.4  
t6.5  
t6.6  
t6.7  
t6.8  
t6.9

t7.1 **Table 7** Model summary  
t7.2 statistics for resistance length  
t7.3 model

Source	Std. dev.	$R^2$	Adj $R^2$	Pred $R^2$	PRESS	
Linear	103.50	0.4776	0.3615	-0.1093	2.047E+005	
2FI	63.25	0.8266	0.7615	0.5788	77734.99	Suggested
Quadratic	55.93	0.8983	0.8135	0.6506	64492.73	
Cubic	30.59	0.9848	0.9442	0.7809	40443.16	Aliased

336 **2.4 Mechanical characterization**

337 Being it impossible to obtain specimens of standard geometry  
338 (to be tested in a common shear stress test) from small size  
339 components as the ones welded in this study, the mechanical  
340 properties of the performed joints are characterized with a  
341 push-out test of the internal martensitic shell with respect to  
342 the outer one. This test practiced on the entire assembled com-  
343 ponents allows for the characterization of the whole seam  
344 (difference in the geometry may appear during the laser power  
345 ramp-up or ramp down). Moreover, the constrained circular  
346 configuration of the weld avoids distortions during the test, as  
347 it often happens from specimen cut from a pressure vessel  
348 (e.g., curvature problems, load misalignment due to the thick-  
349 ness of the shells, etc.).

350 All welding configurations are then tested to shear stresses  
351 under the action of a calibrated press exerting its load on a  
352 specifically conceived expeller. The photographic view in  
353 Fig. 4a shows the setup for the push-out test in which the weld  
354 fails due to the disassembly forces while the model for weld  
355 shear failure is sketched in Fig. 4b: the draft shows the sur-  
356 faces in contact during the test. The load of the press increases  
357 quasi-statically, and the maximum value generating the col-  
358 lapse of the joint (the ultimate shear stress) is recorded.

359 **3 Results and discussion**

360 The effects of individual process parameters (incidence angle  
361 and offset) on geometrical features of the weld cross sections  
362 (resistance length and melting ratio) are plotted by perturba-  
363 tion plots and described in the following sections. To

demonstrate the two-factor interaction effects on the same 364  
weld bead geometry, contour plots are used. Figure 3 shows 365  
typical cross sections and weld profiles in the following: (a) 366  
reference position and (b) the extreme values of the incidence 367  
angle and the offset at the same time. It is possible to see that, 368  
according to the weld design strategy described in Sect. 2.1, 369  
the control of the weld position by a proper selection of input 370  
parameters allows to vary the melting ratio in favor of mar- 371  
tensite or ferrite. 372

**3.1 Visual inspection of weld quality** 373

The reference position welding configuration shows sporadic 374  
superficial defects whose dimensions can be considered ac- 375  
ceptable according to the ISO 13919-1 standard (grade 1). 376  
Results of weld seam inspection are reported in Table 5 as 377  
function of the analyzed weld geometry configurations. Re- 378  
sults show that increasing the incident angle induces higher 379  
ISO 13919 standard numbers, but increasing the offset de- 380  
creases the number and dimensions of microcracks. This 381  
means that the presence of microcracks is mainly driven by 382  
the relative volume fraction of AISI 440C and AISI 430F 383  
steels in the welds. Higher martensitic volume fraction in- 384  
duces higher susceptibility to surface crack formation (tens 385  
of microns length). In fact, microcracks are found to develop 386  
always on the boundary of the weld seam with AISI 440C. 387

**3.2 Ferritic and martensitic width ( $W_F$  and  $W_M$ )** 388

In the reference position, the width at the free surface is nearly 389  
the same for the two materials as it is possible to notice also in 390  
Fig. 3a. Melt pool width on the ferritic side is slightly smaller 391

t8.1 **Table 8** Sequential model sum  
t8.2 of squares for melting ratio model

Source	Sum of squares	$df$	Mean square	$F$ value	$P$ value	Prob> $F$
Mean	14.52	1	14.52			
Linear	7.46	2	3.73	44.42	<0.0001	
2FI	0.55	1	0.55	21.67	0.0016	Suggested
Quadratic	7.083E-003	2	3.542E-003	0.11	0.8993	
Cubic	0.13	3	0.042	1.75	0.3278	Aliased
Residual	0.071	3	0.024	-	-	-
Total	22.74	12	1.90	-	-	-

t9.1 **Table 9** Model summary statistics for melting ratio model

t9.2 Source	Std. dev.	$R^2$	Adj $R^2$	Pred $R^2$	PRESS	
t9.3 Linear	0.29	0.9080	0.8876	0.8032	1.62	
t9.4 2FI	0.16	0.9752	0.9659	0.9420	0.48	Suggested
t9.5 Quadratic	0.18	0.9761	0.9561	0.8979	0.84	
t9.6 Cubic	0.15	0.9913	0.9681	0.8519	1.22	Aliased

392 due to the higher thermal conductivity of AISI 430F with  
 393 respect to AISI 440C (25 and 15 W m<sup>-1</sup> K<sup>-1</sup>, respectively):  
 394 the ED transferred to the material can be easier conducted  
 395 away by the outer shell. This thermal loss makes heat conduction  
 396 anisotropic in the present case. The effect of increasing  
 397 the offset on the melt pool width on both sides (averaged  
 398 values) is shown in Fig. 5 for different incident angles. Increasing  
 399 the offset obviously results in an almost linear increase  
 400 of ferritic width for all the incident angles, conversely for  
 401 the martensitic one. Increasing the incident angle has an opposite  
 402 effect which compensates the asymmetry generated by  
 403 the use of large values of the offset, as hypothesized in  
 404 Sect. 2.1.

405 The base metal microstructures are typically composed by  
 406 a martensitic matrix with presence of primary and secondary  
 407 Cr carbides for the AISI 440C and a ferritic matrix with elongated  
 408 MnS particles for AISI 430F steel.

409 **3.3 Effects of process parameters**

410 To compare the effects of all the process parameters at the  
 411 center point in the design space, the perturbation plot is drawn  
 412 and is shown in Fig. 6a, b. The results suggest that incidence  
 413 angle of laser has the most significant negative impact on both  
 414 the resistance length and MR. For melting ratio, an opposite  
 415 phenomenon of the same entity is observed for the offset: MR  
 416 increases linearly with the increase of offset, and the two linear  
 417 dependencies are found to be symmetric with respect to the  
 418 center point. On the other hand, the resistance length is not  
 419 remarkably affected by the change of offset, at least in the  
 420 tested range.

t10.1 **Table 10** ANOVA table for  
 t10.2 resistance length 2FI model

t10.3 Source	Sum of squares	df	Mean square	F value	P value	Prob>F
t10.4 Model	1.525E+005	3	50849.72	12.71	0.0021	Significant
t10.5 $O$	1128.13	1	1128.13	0.28	0.6098	
t10.6 $A$	87020.42	1	87020.42	21.75	0.0016	
t10.7 OA	64400.62	1	64400.62	16.10	0.0039	
t10.8 Residual	32007.08	8	4000.89			
Cor total	1.846E+005	11				

$R^2 = 0.8266$ , adj  $R^2 = 0.7615$ , pred  $R^2 = 0.5788$ , adeq precision = 12.85

Figure 7a shows the contour plot for resistance length as a  
 function of interaction between offset and angle. For the initial  
 two levels of  $A$  (0° and 15°),  $S$  increases with the increase of  $O$   
 while the opposite phenomena are observed for the other two  
 levels of  $A$ .

Contour plots as shown in Fig. 7b demonstrate the fact that  
 interactions of higher offset and lower incidence angle of laser  
 cause higher melting ratio. In the reference position, the averaged  
 melting ratio on the three weld specimens results MR = 0.8: this  
 value is lower than one which theoretically represents a condition  
 of symmetry with respect to the interface between the two materials.  
 Actually, the ferritic area results smaller than the martensitic one  
 for all the three samples tested in the same condition. This  
 phenomenon can be traced back to the already mentioned higher  
 thermal conductivity of AISI 430F which favors heat conduction  
 away from the irradiated area. As a result, the melt pool develops  
 more on the AISI 440C area and makes this material, which is also  
 characterized by a much more brittle microstructure, more  
 susceptible to cracking. Thus, it should be taken into account  
 that even in a symmetric configuration, like the reference position,  
 the weld pool develops in asymmetric way due to the different  
 thermal properties of the two dissimilar metals. MR increases  
 almost linearly with the offset for each incidence angle: it  
 especially increases faster for 0° and 15° for which the percentage  
 of melt ferrite more than doubles. For the higher values of  $A$ ,  
 the direction of the beam axis, pointing to the martensitic steel,  
 compensates the effect of the offset and the rate of growth of  
 the ferritic area is less pronounced.

**3.4 Development of mathematical models**

At this stage, the fit summary in the Design-Expert software  
 V7 is used to select the models that best describe the response  
 factors. The fit summary includes sequential model sum squares  
 to select the highest order polynomial where additional terms  
 are significant and the model is not aliased. In addition,  
 model summary statistics of the fit summary focuses on the  
 model that maximizes adjusted  $R^2$  and predicted  $R^2$  values.  
 The sequential F test and lack-of-fit test are carried out using  
 the same statistical software package to check if the regression



t11.1 **Table 11** ANOVA table for  
t11.2 melting ratio 2FI model

	Source	Sum of squares	df	Mean square	F value	P value Prob>F	
t11.3	Model	8.02	3	2.67	104.87	<0.0001	Significant
t11.4	<i>O</i>	3.51	1	3.51	137.81	<0.0001	–
t11.5	<i>A</i>	3.95	1	3.95	155.13	<0.0001	–
t11.6	<i>OA</i>	0.55	1	0.55	21.67	0.0016	–
t11.7	Residual	0.20	8	0.025	–	–	–
t11.8	Cor total	8.22	11	–	–	–	–

$R^2 = 0.9752$ ,  $adj R^2 = 0.9659$ ,  $pred R^2 = 0.9420$ ,  $adeq\ precision = 31.088$

460 model is significant and to find out the significant model terms  
461 of the developed models as well. The stepwise regression  
462 method is also applied to eliminate the insignificant model  
463 terms automatically.

464 Suitable response models for the response factors are selected  
465 based on the fit summaries. From fit summary output of  
466 the measured responses shown in Tables 6, 7, 8, and 9, it is  
467 evident that two-factor interaction (2FI) models are statistical-  
468 ly recommended for further analyses of both the resistance  
469 length and melting ratio.

470 The test for significance of the regression models and the  
471 test for significance on individual model coefficients are per-  
472 formed using the same statistical package. By selecting the  
473 stepwise regression method that eliminates the insignificant  
474 model terms automatically, the resulting ANOVAs in  
475 Tables 10 and 11 for the selected models summarize the  
476 ANOVA of each response and illustrate its significant model  
477 terms as well. The aforesaid tables demonstrate that calcu-  
478 lated Fisher’s “Model-F” and “Model-P” values are, respec-  
479 tively, 12.71 and 0.0021 for resistance length’s 2FI model and  
480 104.87 and <0.0001 for melting ratio 2FI model. These  
481 Model-F and Model-P values imply that the selected models  
482 are highly significant and there is only 0.21 % and a less than

0.01 % chance that these large Model-F values could occur  
due to noise. The associated P value is also used to estimate  
whether F is large enough to indicate statistical significance. If  
P value is lower than 0.05, it indicates that the model is sta-  
tistically significant as stated by Zulkali et al. [24].

Tables 10 and 11 also show other adequacy measures, e.g.,  
 $R^2$ , adjusted  $R^2$ , and predicted  $R^2$  values. All the adequacy  
measures are in logical agreement and indicate significant  
relationships. Moreover, adequate precision compares range of  
predicted value at the design points to average prediction  
error. The adequate precision ratios in all cases are dramati-  
cally greater than 4 indicating adequate model discrimination.  
Again, the ANOVA tables for the resistance length model and  
melting ratio model show that all two linear terms, i.e., offset  
and laser incident angle and two-factor interactions (2FI) of  
offset-angle (*O-A*), are significant model terms. From the re-  
sults shown in Tables 6, 7, 8, 9, 10, and 11, it is, therefore,  
apparent that the developed statistical models for predicting  
resistance length and melting ratio are fairly accurate and can  
be of following forms:

$$1. \text{ Resistance length, } S = 523.75 - 11.87 \times O - 114.25 \times A + 120.37 \times O \times A$$

**Fig. 8** Normal probability plot for a resistance length and b melting ratio

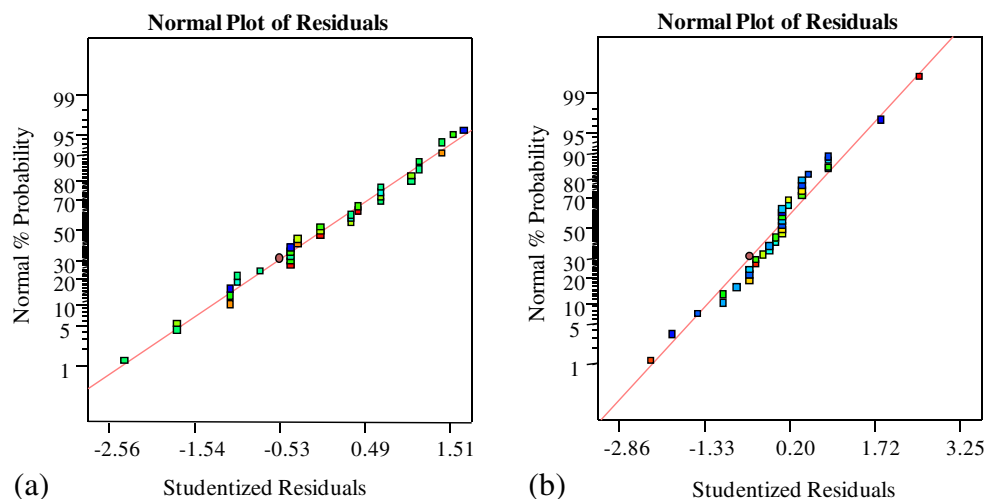
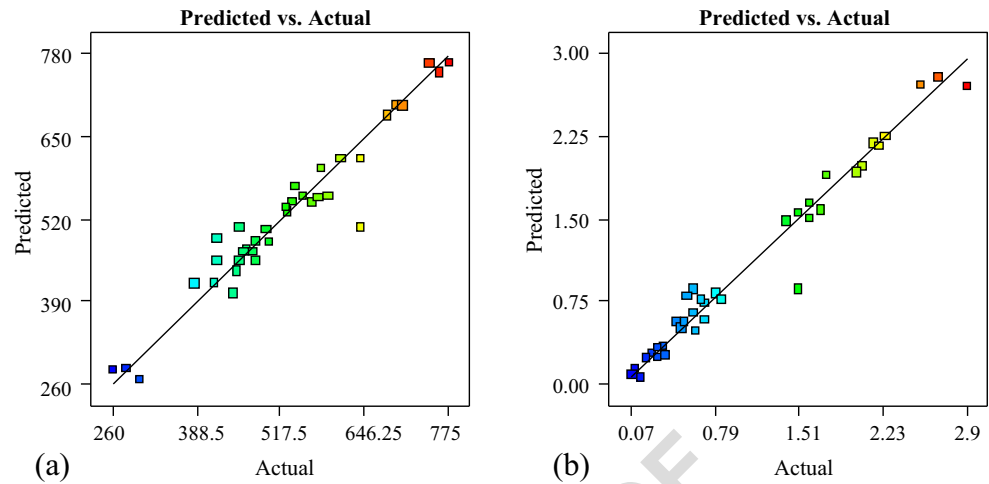


**Fig. 9** Scatter diagrams of **a** resistance length and **b** melting ratio



505 2. Melting ratio,  $MR = 1.1 + 0.66 \times O - 0.77 \times A - 0.35 \times O \times A$

506 Normality of residual data and amount of residuals in pre-  
 507 diction are then checked to ensure statistical validation of the  
 508 developed models. The normality of data is verified by plotting  
 509 the normal probability plot (NPP) of residuals. The residual  
 510 is the difference between observed and predicted values  
 511 (or fitted value) obtained from the regression model. The data  
 512 set is normally distributed if the points on the plot fall fairly  
 513 close to the straight line. The NPPs of residual values for weld  
 514 resistance length and melting ratio are depicted in Fig. 8a, b,  
 515 respectively. The experimental points are reasonably aligned

with predicted or fitted points suggesting the normality of  
 data. This is an implication that empirical distribution of residual  
 data is well compared with a normal distribution having the same  
 mean and variance.

Figure 9a, b shows the relationships between the actual and  
 predicted values of weld resistance length and melting ratio.  
 Since the points plotted are close to and around the diagonal  
 line, the difference between the predicted and actual values for  
 each point can be considered to be minimal. It is also an  
 indication that the statistical models for prediction are adequate  
 and predicted results are in good agreement with the measured  
 data.

t12.1 **Table 12** Summary of results of investigated parameters

t12.2	Welding configuration	Averaged melting ratio, MR (a.u.)	Carbon in melting pool (%)	Averaged resistance length, S (μm)	Surface cracks <sup>a</sup>	Averaged USF (N)
t12.3	1	0.8	0.66	760	1	4900
t12.4	2	2.0	0.45	695	0	4380
t12.5	3	2.7	0.38	465	0	4180
t12.6	4	0.5	0.77	535	3	3825
t12.7	5	1.6	0.49	610	0	4200
t12.8	6	2.2	0.43	450	0	4020
t12.9	7	0.3	0.87	480	3	3550
t12.10	8	0.6	0.73	550	2	3940
t12.11	9	1.5	0.51	590	0	4540
t12.12	10	0.1	1.01	280	3	2710
t12.13	11	0.3	0.87	415	3	3650
t12.14	12	0.6	0.73	455	2	4090

All data refer to the average value of three specimens. Values are attributed according to ISO 13919-1:1996 [17], after inspection on the three samples for each configuration

<sup>a</sup> 0=no defects, 1=exist but acceptable, 2-3=not acceptable

### 3.5 Ultimate shear force

The value of the ultimate force making the weld collapsing under shear stresses, averaged for the three tested samples, is reported in Table 12 along with all the other investigated parameters (S, MR, crack grade). All failure data reported in Table 12 (under the column “Averaged ultimate shear force (USF)”) are related to a brittle fracture of the weld. The applied load increases quasi-statically with increasing the application time up to the moment in which the fracture propagates drastically over the 360° detaching the two components.

The averaged MR gives an indication of the carbon content of the fusion zone (also reported in the table), where the chemical composition is the average between the two base steels weighted for their volume fraction. This is because, as reported in Table 1, the other main element (chromium, manganese, and silicon) concentrations are almost the same for the two welded steels; thus, the properties of the melting pool are driven by the carbon content. It ranges between 0.4 and 1 % for the highest and lowest measured MR values, respectively.

According to the literature [15, 25], the USF linearly depends on the dimension of the resistance length. The highest

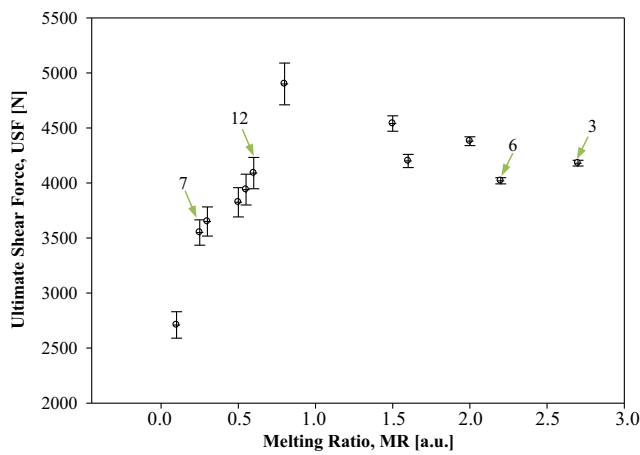


**Fig. 10** Ultimate shear force of the fusion zone as a function of melting ratio

USF is then obtained in the reference position for which the resistance length has the highest value within the tested range.

Nevertheless, a second important effect on USF can be also noticed referring to those configurations having a nearly same resistance length but different melting ratio. Considering only the linear dependence of USF on the resistance length, those configurations having a similar  $S$  ( $\pm 10 \mu\text{m}$ ) should break under a similar load. Conversely, Table 12 shows that configurations 3 and 6 result in a sensible higher USF in respect to 7 and 12 for which the percentage of martensitic material in the melt pool is higher.

Figure 10 representing the behavior of USF as a function of the melting ratio obviously includes also the dependence on  $S$ . In order to give evidence on how the melting ratio influences the USF, couples of welding configurations having the same  $S$

but different MR have to be considered. As an example, welding configuration numbers 3 and 6 (see Table 12) with  $MR=(2.7-2.2)$ , respectively, and  $S=(450-460)\mu\text{m}$  can be compared to numbers 7 and 12 (obtained with large  $A$ ):  $S=(450-480 \mu\text{m})$  but opposite  $MR=(0.3-0.6)$  as indicated by arrows in Fig. 10. Measured data reveal that increasing the volume fraction of the ferritic stainless steel in the melt pool has beneficial aspects on the ultimate shear strength. Also, data dispersion (with respect to the averaged value reported in Table 12) decreases with increasing MR, making the failure mode more predictable. This means that the prevailing effect is the decreased brittleness of the weld by decreasing its carbon content. In fact, high carbon content in the melt pool not only increases the crack susceptibility but also lowers the USF.

Experimental results suggest the use of welding configurations generating  $MR \geq 1.5$  to obtain a crack-free surface (grade 0 according to the ISO 13919-1 standard) and to ensure high and well-reproducible USF.

An attempt to link mathematically the USF to the parameters which determine the welding configuration is developed by means of the full factorial DOE.

$$USF = 1408.18 + 4778.52 \times O + 940.85 \times A - 1562.99 \times O \times A$$

The NPP of residual values for USF is depicted in Fig. 11. The experimental points are reasonably aligned with predicted or fitted points suggesting the normality of data. This is an implication that empirical distribution of residual data is well compared with a normal distribution having the same mean and variance.

Figure 12 shows the relationships between the actual and predicted values of weld USF. Since the points plotted are close to and around the diagonal line, the difference between the predicted and actual values for each point can be

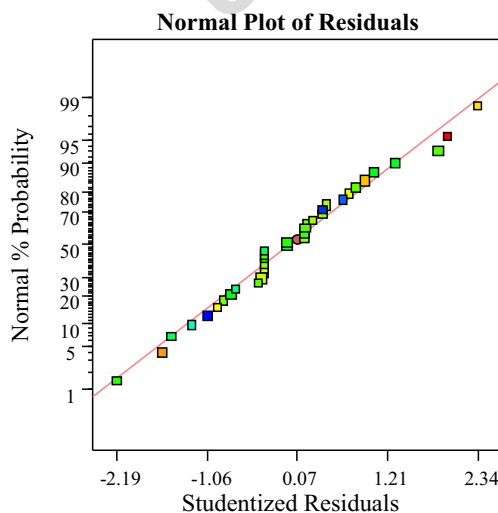


**Fig. 11** Normal probability plot weld USF

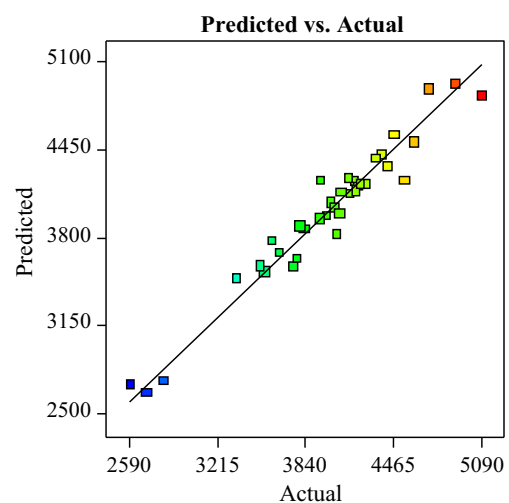


**Fig. 12** Scatter diagram of USF

599 considered to be minimal. From Fig. 12, it is clear that the  
 600 predicted results are in good agreement with the measured  
 601 data for USF.

602 **4 Conclusions**

603 Ferritic AISI 430F and martensitic AISI 440C stainless steel  
 604 shells have been laser welded in constrained butt configura-  
 605 tion. The effects of different combination of incident angles  
 606 and offsets have been studied, analyzing the following param-  
 607 eters of the fusion zone: cross-sectional geometry (resistance  
 608 length and width at the free surface), melting ratio between the  
 609 dissimilar steels, presence of surface cracks and relative di-  
 610 mensions, and ultimate shear strength of the welds. For the  
 611 laser system, weld joint type, and the limits of laser parameters  
 612 considered in this study, the following points can be  
 613 concluded:

614 The presence of surface cracks is more relevant when the  
 615 melting ratio is lower than 0.8 (reference position). This is  
 616 more evident with incident angles of 30° and 45°, al-  
 617 though some mitigations could be obtained by increasing,  
 618 at the same time, the offset value. It was shown that the  
 619 welding configuration controls the geometry of the weld  
 620 and the mixing between the dissimilar steels which influ-  
 621 ences strength and brittleness of the seam.

622 Both resistance length and melting ratio can be readily  
 623 linked to laser offset and incidence angle at the shell  
 624 interface by using a linear regression over the experimen-  
 625 tal data. Remarkably, the melting ratio is a good indicator  
 626 of the carbon content on the fusion zone and the critical  
 627 value MR=1.5 is related to carbon content in the fusion  
 628 zone of about 0.5 %.

629 Well-reproducible USF in the range of 4.5–4 kN can be  
 630 obtained with welding configurations generating MR  
 631  $\geq 1.5$  with an almost negligible incidence of surface  
 632 cracks (grade 0 according to the ISO 13919-1 standard).  
 633 It was proved that the ultimate shear strength is not only  
 634 linearly dependent on the resistance length but also sus-  
 635 ceptible to the micromechanical properties of fusion zone  
 636 (especially brittleness) and, thus, to the melting ratio.  
 637 Measured data revealed that it is possible to find an em-  
 638 pirical relationship between the shear strength of the weld  
 639 and the configuration adopted during experiments by  
 640 using full factorial DOE.

641 These conclusions pinpointed for the welding conditions  
 642 under investigation can be easily extended to a broader range  
 643 of weld designs under the limiting condition that the forma-  
 644 tion of the weld bead is conduction dominated and plasma forma-  
 645 tion is not considered.

**Acknowledgements** Maria Carmela Fierro, laser-welding expert at  
 Continental Automotive Italy s.p.a., is sincerely acknowledged for pro-  
 viding means and facilities needed to carry out the experimental phase.

**References**

1. Messler WRJ (2004) Joining of metals, alloys, and intermetallics. *Joi Mater Struct* pp. 535–582

2. Wenyong W, Shengsun H, Shen J (2015) Microstructure, mechanical properties and corrosion behavior of laser welded dissimilar joints between ferritic stainless steel and carbon steel. *Mater Des* 65:855–861

3. Phanikumar G, Manjini S, Dutta P, Mazumder J, Chattopadhyay K (2005) Characterization of a continuous CO<sub>2</sub> laser-welded Fe-Cu dissimilar couple. *Metall Mater Trans A* 36A:2137–2147

4. Sun Z, Ion JC (1995) Laser welding of dissimilar metal combinations. *J Mater Sci* 30:4205–4214

5. Duley WW (1999) Laser welding. Wiley, New York

6. Vaidya WV, Horstmann M, Ventzke V, Petrovski B, Kocak M, Kocik R, Tempus G (2010) Improving interfacial properties of a laser beam welded dissimilar joint of aluminium AA6056 and titanium Ti6Al4V for aeronautical applications. *J Mater Sci* 45:6242–6254

7. Chen L, Zhou L, Tang C, Huang W, Wang C, Hu X, Wang J, Yan F, Wang X, Jiang Z, Shao X (2014) Study of laser butt welding of SUS301L stainless steel and welding joint analysis. *Int J Adv Manuf Technol* 73:1695–1704

8. Caiazzo F, Alfieri V, Sergi V, Schipani A, Cinque S (2013) Dissimilar autogenous disk-laser welding of Haynes 188 and Inconel 718 superalloys for aerospace applications. *Int J Adv Manuf Technol* 68:1809–1820

9. Gao M, Wang ZM, Li XY, Zeng XY (2012) Laser keyhole welding of dissimilar Ti-6Al-4V titanium alloy to AZ31B magnesium alloy. *Metall Mater Trans A* 43A:163–172

10. Berretta JR, de Rossi W, Neves MDM, de Almeida IA, Junior NDV (2007) Pulsed Nd:YAG laser welding of AISI 304 to AISI 420 stainless steels. *Opt Lasers Eng* 45:960–966

11. Liao YC, Yu MH (2007) Effects of laser beam energy and incident angle on the pulse laser welding of stainless steel thin sheet. *J Mater Process Technol* 190:102–108

12. Benyounis KY, Olabi AG (2008) Optimization of different welding processes using statistical and numerical approaches—a reference guide. *Adv Eng Softw* 39:483–96

13. Anawa EM, Olabi AG (2008) Optimization of tensile strength of ferritic/austenitic laser-welded components. *Opt Lasers Eng* 46: 571–577

14. Ruggiero A, Tricarico L, Olabi LG, Benyounis KY (2011) Weld-bead profile and costs optimisation of the CO<sub>2</sub> dissimilar laser welding process of low carbon steel and austenitic steel AISI316. *Opt Laser Technol* 43:82–90

15. Khan MMA, Romoli L, Fiaschi M, Dini G, Sarri F (2012) Multiresponse optimization of laser welding of stainless steels in a constrained fillet joint configuration using RSM. *Int J Adv Manuf Technol* 62:587–603

16. Marashi P, Pouranvari M, Amirabdollahian S, Abedi A, Goodarzi M (2008) Microstructure and failure behavior of dissimilar resistance spot welds between low carbon galvanized and austenitic stainless steels. *Mater Sci Eng A* 480:175–180

17. Torkamany MJ, Sabbaghzadeh J, Hamed MJ (2012) Effect of laser welding mode on the microstructure and mechanical performance of dissimilar laser spot welds between low carbon and austenitic stainless steels. *Mater Des* 34:666–672

- 707 18. Rossini M, Russo Spena P, Cortese L, Matteis P, Firrao D (2015) 720  
708 Investigation on dissimilar laser welding of advanced high strength 721  
709 steel sheets for the automotive industry. *Mater Sci Eng A* 628:288– 722  
710 296  
711 19. Baghjari SH, AkbariMousavi SAA (2014) Experimental investiga- 723  
712 tion on dissimilar pulsed Nd:YAG laser welding of AISI 420 stain- 724  
713 less steel to kovar alloy. *Mater Des* 57:128–134  
714 20. Franco A, Romoli L, Musacchio A (2014) Modelling for predicting 725  
715 seam geometry in laser beam welding of stainless steel. *Int J Therm* 726  
716 *Sci* 79:194–205  
717 21. ISO 13919-1:1996 Welding—electron and laser-beam welded 727  
718 joints—guidance on quality levels for imperfections—part 1: steel 728  
719 (reviewed in 2011). 729  
733 22. Serizawa H, Mori D, Shirai Y, Ogiwara H, Mori H (2013) 730  
Weldability of dissimilar joint between F82H and SUS316L under 731  
fiber laser welding. *Fusion Eng Des* 88(9-10):2466–2470 732  
23. Rai R, Elmer JW, Palmer TA, DebRoy T (2007) Heat transfer and 723  
fluid flow during keyhole mode laser welding of tantalum, Ti–6Al– 724  
4V, 304L stainless steel and vanadium. *J Phys D Appl Phys* 40: 725  
5753–5766 726  
24. Zulkali MMD, Ahmad AL, Norulakmal NH (2006) *Oryza sativa* L. 727  
husk as heavy metal adsorbent: optimization with lead as model 728  
solution. *Bioresour Technol* 97:21–25 729  
25. Khan MMA, Romoli L, Fiaschi M, Dini G, Sarri F (2012) Laser 730  
beam welding of dissimilar stainless steels in a fillet joint configu- 731  
ration. *J Mater Proc Technol* 212:856–867 732

UNCORRECTED PROOF



AUTHOR QUERY

**AUTHOR PLEASE ANSWER QUERY.**

No Query.

UNCORRECTED PROOF